electronics

MDPI

Article

EMC Impact of Disturbances Generated by Multiple Sources

Hamidreza Karami [1,2,*], Marcos Rubinstein [3], Farhad Rachidi [1], Christophe Perrenoud [4], Emmanuel de Raemy [4], Pascal Kraehenbuehl [4] and Arturo Mediano [5]

1 Electromagnetic Compatibility Laboratory, Ecole Polytechnique Fédérale de Lausanne (EPFL), 1015 Lausanne, Switzerland
2 Department of Electrical Engineering, Bu-Ali Sina University, Hamedan 65178-38695, Iran
3 Institute for Information and Communication Technologies, University of Applied Sciences and Arts Western Switzerland (HES-SO), 1401 Yverdon-les-Bains, Switzerland
4 Electromagnetic Compatibility Section, Swiss Federal Office of Communications (OFCOM), 2503 Biel/Bienne, Switzerland
5 Engineering Research Institute of Aragon (I3A), University of Zaragoza, 50009 Zaragoza, Spain
* Correspondence: hamidreza.karami@epfl.ch; Tel.: +41-21-693-48-18

Abstract: In this paper, the impact of an increasing number of arbitrary electrical/electronic devices on the overall radiated emissions is investigated. Understanding and quantifying such an impact are prerequisites to the proper evaluation of electromagnetic compatibility (EMC) of various electronic systems and devices and, if needed, to revisiting the international standards. To evaluate the radiated emissions from multiple electronic devices, each arbitrary electronic device is characterized using an equivalent Huygens's surface, in which the tangential components of electric and magnetic near fields are calculated (or measured). The radiated emission from the arbitrary electronic device can be calculated using the electric and magnetic near fields for an arbitrary phase (correlated or uncorrelated), position, and orientation. The influence of several parameters affecting the radiated emissions from multiple arbitrary electronic devices, including the number of disturbance sources, the polarization of each device, the radiation pattern of each device, the location and orientation of each device, and the phase shifts between devices, are analyzed. The numerical results show that the mentioned parameters have a significant effect on the radiated emissions, and cannot be neglected in EMC considerations. In general, increasing the number of electronic devices leads to an increase in the level of radiated emissions. However, the increase depends on other parameters such as the arrangement (the radiation pattern for each device, the distance between the devices, and the orientation and/or polarization of each device). The proposed method can be straightforwardly applied to devices characterized by near-field measurements or multimodular large equipment with long cables.

Keywords: electromagnetic interference (EMI) sources; multiple sources; Huygens's principle; near-field measurements; Monte Carlo simulation; stochastic electromagnetic interference calculation; electromagnetic compatibility (EMC); emission limits

Citation: Karami, H.; Rubinstein, M.; Rachidi, F.; Perrenoud, C.; de Raemy, E.; Kraehenbuehl, P.; Mediano, A. EMC Impact of Disturbances Generated by Multiple Sources. *Electronics* **2022**, *11*, 3530. https://doi.org/10.3390/electronics11213530

Academic Editor: Paolo Stefano Crovetti

Received: 19 September 2022
Accepted: 25 October 2022
Published: 29 October 2022

1. Introduction

The pervasive use of electronic devices operating at high frequencies (such as mobile phones, laptops, notepads, etc.) can lead to an increase in the level of unwanted radiated emissions, i.e., electromagnetic interference (EMI) [1,2]. If the radiated emissions from electronic devices exceed some critical value, the performance of other electronic equipment in its vicinity can be degraded. To avoid these situations, the maximum conducted and radiated emissions from electronic devices are restricted by electromagnetic compatibility (EMC) standards [3]. EMC testing is generally carried out considering only a single device. However, the significant increase in electronic devices used nowadays might result in an increase in the overall noise floor and affect the immunity of neighboring devices and

systems. As a result, the subject of the impact of an increasing number of devices on the overall emissions has attracted some attention recently [4–9], and it is currently being discussed within international standardization bodies (e.g., Comité International Spécial des Perturbations Radioélectriques (CISPR)). Understanding and quantifying such an impact are prerequisites to the proper evaluation of EMC of various electronic systems and devices and, if needed, to revisit international standards.

In the study by Takahashi et al. [5], it was shown that by increasing the number of devices, the radiated emissions will increase. The assumed geometry of the problem in [5] was a linear array of current sources. The distance between the array elements was constant and equal to d. Each array element had the same amplitude but with a randomly varied phase between 0 to 2π rad. The maximum radiated emissions for all observation points with a height of 1 to 4 m and with steps of 0.3 m above the ground was calculated and compared with the maximum radiation of a single device. The results show that by allowing the phase to vary from 0 to 2π rad, the radiated emissions from multiple devices are reduced from the voltage sum obtained for a constant and equal phase for all radiators (the same as the electric field sum) to the power sum curve. In the same paper [5], the phase variation for large telecommunication equipment was measured, and it was shown that the assumption of a randomly varied phase between 0 to 2π rad is valid. Finally, to check the validity of the random phase assumption, two experimental case studies including three spherical dipole antennas and actual large telecommunication equipment were presented. It was concluded that the radiated emission from multiple devices agreed well with the power sum formula when each element has a randomly varied phase between 0 to 2π rad. Note that in [5], all of the considered devices were identical and represented by simple isotropic patterns. They were also configured in a linear array and had fixed orientations.

Häberlin [6] also used the power sum formulation assuming a 2π rad random phase variation for the different devices. The disturbance sources were modeled as noise with uncorrelated distribution over their operating frequency range. The victim was considered to be a simple dipole antenna, and the received power from each source was calculated using

$$P = cos(\alpha)/R \tag{1}$$

where R and $cos(\alpha)$ are, respectively, the magnitude of the source-to-observation radial spherical vector and the cosine of the angle between the Poynting vector and the effective area of the simple dipole antenna.

The total disturbance power P_t at a y-polarized virtual dipole in the origin due to nearby uncorrelated isotropic disturbance sources placed in a two-dimensional square grid (the area of each mesh in the grid is 1×1 m^2) was calculated using (1) and the superposition theorem. The increased disturbance level G_n was calculated by dividing the total disturbance by the disturbance power from only one disturbance source P_1 at a distance D = 1 m in [6], i.e., $G_n = P_t/P_1$. For example [6], according to CISPR 11, at a measuring distance of 10 m, the limit for the electric field radiated emissions is 30 dBμV/m at 30 MHz for class-B devices. If there are many such devices (for example n = 30) making full use of these limits within a distance of 300 m, G_n = 12 dB can be obtained. This means that instead of the allowed 30 dBμV/m, the resulting radiation will be 42 dBμV/m. Note that this method was extended in [6] to a three-dimensional distribution of the disturbance sources. The analysis approach for the three-dimensional distribution is similar to the two-dimensional cases. In a 121 × 121 grid with 14,640 interference sources (in this case, the center element was removed), the relative increase in the disturbance power was 18.02 in linear units, which equals 12.56 dB. In the case of a three-dimensional distribution, realized by way of distributed sources in six layers (six floors), the relative increase in the radiated emissions for a 2 m long vertical antenna representing the victim was between 13 and 17 dB [6]. Note that Häberlin [6] considered an isotropic pattern to model the radiated emissions from each of the devices, which is not a realistic assumption. The calculations in [6] were performed considering a specific victim, namely a vertical dipole antenna. The multiple sources were considered uncorrelated.

In [7], the impact of an increasing number of devices was investigated numerically and experimentally. Using numerical simulations, a comparison between the electric field strength of one antenna dipole and ten similar dipoles was examined. In this simulation, all ten antenna dipoles were on the perimeter of a circle located at a height of 2 m above a perfect electric plane. This setup was chosen to keep the distance between the victim (at the origin of the coordinate system) and each source the same. Note that the distance chosen in this study is 10 m, which is the protection distance used for most CISPR publications in residential environments. The dipoles represent uncoupled disturbance sources emitting, however, at the same frequency. A free method-of-moments-based simulation tool (Numerical Electromagnetic Code (NEC)-2) was used to calculate the radiated emissions from the dipole(s) fed by a 100 V voltage source with a random phase. For an arithmetical comparison of the setup, the electric field strength in the midpoint of both setups at a height of h = 2 m was evaluated for the frequencies f_1 = 1 MHz, f_2 = 7 MHz, and f_3 = 30 MHz. The increase in radiated emissions from one dipole to ten dipoles was about 18 dB, independent of the frequency.

In the same report [7], the radiated emissions for an array of "universal laptop power supplies" and "LED chain of lights" with five elements in each case were measured. The abbreviation LED stands for light-emitting diode. The difference between the radiated emissions of an array of "universal laptop power supplies" with five elements and a single element was determined for the frequency range from 30 to 150 MHz. It was shown that the increase in the field strength at the victim location was slightly less than 10 dB on average. The same procedure was also applied for the "LED chain of lights". In this case, the difference between the radiated emissions of an array of "LED chains of lights" with five elements and a single element was determined for the frequency range from 30 MHz to 220 MHz. The resulting increase in the field strength at the victim location was between 5 to 8 dB. Note that in [7], the same elements (dipole antennas) were used to model the multiple devices when evaluating the radiated emissions.

In [8], a method similar to that in [5] was used to evaluate the radiated emission of fully mounted intermodular networking equipment containing tens of nearly identical line cards and hundreds of optical modules. The results show that when the optical modules in one line card are operating at the same frequency, the total radiated field strength can be estimated by multiplying the radiation pattern of a single module by the array factor [10]. However, when a system has multiple uncorrelated sources radiating at slightly different frequencies, the total electric field strength can be estimated using the power sum formula presented in [5].

In [9], a real-world product with various double data rate (DDR) memory modules and highspeed connectors was studied. This study used a vector network analyzer (VNA) in tuned receiver mode to measure the phase for the random DDR sources around the assumed Huygens' box. The highspeed connector was reconstructed using an equivalent dipole. The total contribution of the Huygens' box and the equivalent dipole were further studied based on their uncorrelated relationship. The simulated radio frequency interference (RFI) using the reconstructed model agreed well with the measured RFI from these random noise sources, with a deviation of less than 5 dB. Furthermore, the intermodular effects of the radiation from multiple random noises were considered.

The shortcomings of the reviewed studies can be summarized as follows: (a) the same elements were used to model the multiple devices when calculating the radiated emissions [5–8]; (b) the same isotropic pattern was used to model each device's radiated emissions [5,6]; (c) all the sources were considered uncorrelated [5–7], so the power sum formula could have been used; (d) all the devices were located in a predefined 2D/3D regular grid, with a constant separation distance of 1 m between adjacent devices [6]; (e) the calculations were performed assuming a specific victim, namely, a vertical dipole located at the center of the volume [6]. It appears that published studies [5–9] on the topic at hand are largely based on simplifying assumptions, such as isotropic sources or predetermined placement of the devices.

Compared to the reviewed studies [5–9], the main advantages of the proposed method in the present paper are as follows:

- The proposed method uses the surface equivalent theory to calculate the electric and magnetic current densities (or fields) on a rectangular cuboid around each EMI source. This method allows any arbitrary number of different devices with different radiation patterns to be used to estimate the radiated emissions.
- The locations and orientations of each EUT can be randomly selected. The proposed method does not have any restrictions on this point. After calculating the electric and magnetic current densities (or fields) for each source, these current densities (or fields) can be randomly positioned and/or rotated.
- Unlike the simulations performed in [5,6], in which the orientation of the devices was ignored when calculating the total power radiation, in the proposed approach the effect of the orientation of each EUT can be easily included in the evaluation of the radiated emissions.
- The proposed method can estimate the far-field radiated emissions for a wide frequency range. In other words, the effect of the frequency can be included in the far-field estimations, unlike any of the previous approaches [5–9].

In this paper, the estimation method is complemented and generalized by taking new parameters into account. Table 1 presents a comparison between the methods used in the reviewed studies [5–9] to evaluate the radiated emissions from multiple devices. The last row of the table presents the characteristics of the proposed method.

Table 1. Comparison of the presented methods to evaluate the radiated emissions from multiple devices.

	Pattern	Placement and Orientation	Phase	Measurements	Theory
Takahashi et al. [5]	isotropic	predefined	uncorrelated	included	power sum
Häberlin [6]	isotropic	predefined	uncorrelated	not included	power sum
Kootz and Kiwull [7]	dipole	predefined	uncorrelated	included	power sum
Ghosh et al. [8]	slot	predefined	either correlated or uncorrelated	included	array formula
Zhang et al. [9]	arbitrary	predefined	uncorrelated	included	SRT [1]
This paper	arbitrary	random	arbitrary [2]	not included	SRT

[1] Source reconstruction techniques. [2] One can impose the phase of each device.

The rest of the paper is organized as follows. In Section 2, a new method to calculate the maximum radiated emissions from multiple devices using surface equivalence theory is presented. The proposed method can be used to model any number of different devices with an arbitrary pattern or assumed phases. Both correlated and uncorrelated devices can be simulated using this method. Additionally, the locations and orientations of the devices can also be randomly selected. By considering these assumptions, a realistic setup can be modeled. A simulation method for evaluating radiated emissions from multiple sources considering their stochastic nature is developed. Section 3 presents several examples of the application of the proposed method. General conclusions are presented in Section 4.

2. Methods: Application of the Surface Equivalence Theorem

Generating a full-wave solution of Maxwell's equations [11–14] for a single, real-world EMI source can be a time-consuming task. It can become prohibitive if the calculations are conducted for multiple EMI sources (see Section 2.3 for more information). To cope with this problem, the surface equivalence theorem is applied to each EMI source, and the equivalent surface current densities on a rectangular cuboid around the EMI source are calculated. Then, applying the superposition theorem, the radiated emission from the multiple EMI sources is calculated. Using the equivalent surface current densities for each EMI source has the following advantages:

- The full-wave solution of Maxwell's equations for each EMI source is calculated only once in the determination of the equivalent sources. Alternatively, the near-field

measurements to obtain the equivalent surface current densities of the real-world EMI source can be performed once.
- Translation, rotation, assumed phase of the EMI sources, and changes in the observation point(s) do not affect the distribution of the equivalent surface current densities.
- The equivalent surface current densities can be calculated or measured on an arbitrarily shaped surface, which can be determined based on the considered device (EMI source).
- The total radiated emissions from multiple EMI sources can be easily calculated analytically by considering the equivalent surface current densities of each EMI source simultaneously.

The application of the surface equivalence theorem to calculate the equivalent surface current densities for each EMI source is detailed in the following subsections.

2.1. Theory of Surface Equivalence for a Single EMI Source

Using the surface equivalence theorem, the actual arbitrary EMI source is replaced by an equivalent source that produces the same electromagnetic fields in the region of interest. An arbitrary EMI source, such as the printed circuit board (PCB) shown in Figure 1a, is considered. The assumed PCB in Figure 1a radiates electric and magnetic fields $\boldsymbol{E}_1$ and $\boldsymbol{H}_1$. A closed surface S, which, in general, can have an arbitrary shape, encloses the assumed PCB, as shown in Figure 1a. The volume within the surface S is denoted by V_1 and the volume outside the surface S is denoted by V_2. Note that in this paper, without loss of generality, the surface S is assumed to be a rectangular cuboid. This makes it easier to capture the tangential components of the electric and magnetic fields in both numerical simulations and experimental measurements.

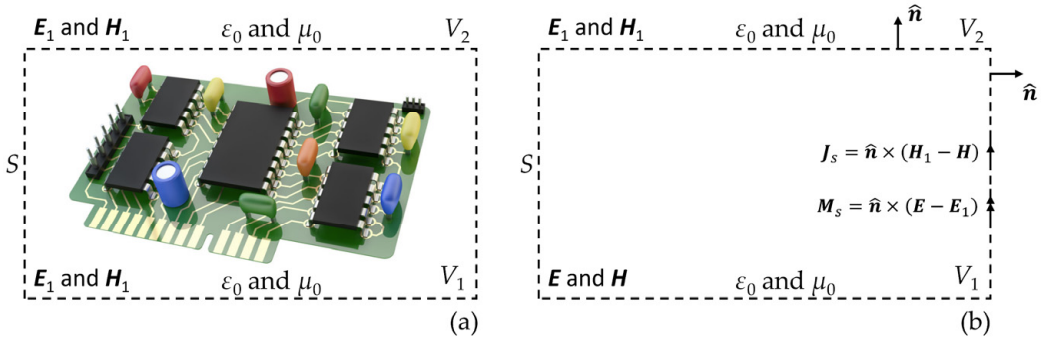

Figure 1. The geometry of the problem: (**a**) actual arbitrary PCB, (**b**) the equivalent problem model.

Applying the surface equivalence theorem, the equivalent problem of Figure 1a is shown in Figure 1b. The original EMI source (the assumed PCB) is removed. Note that the fields ($\boldsymbol{E}$ and $\boldsymbol{H}$) are assumed inside surface S and the fields ($\boldsymbol{E}_1$, $\boldsymbol{H}_1$) outside the surface S. For these fields to exist within and outside S, they must satisfy the boundary conditions on the tangential electric and magnetic field components. Thus, on the virtual surface S, there must exist equivalent sources [10,15],

$$\boldsymbol{J}_s = \hat{\boldsymbol{n}} \times (\boldsymbol{H}_1 - \boldsymbol{H}) \tag{2}$$

$$\boldsymbol{M}_s = \hat{\boldsymbol{n}} \times (\boldsymbol{E} - \boldsymbol{E}_1) \tag{3}$$

where $\hat{\boldsymbol{n}}$ denotes the normal outward vector to the surface S. The surface current densities radiate in an unbounded space (V_2). The current densities ($\boldsymbol{J}_S$ and $\boldsymbol{M}_S$) of Equations (2) and (3) are equivalent only within V_2, because they produce the original field ($\boldsymbol{E}_1$, $\boldsymbol{H}_1$) only outside the surface S. Fields ($\boldsymbol{E}$, $\boldsymbol{H}$), different from the original ($\boldsymbol{E}_1$, $\boldsymbol{H}_1$), are produced within V_1. Since the fields ($\boldsymbol{E}$, $\boldsymbol{H}$) are not important in this paper, they are set to zero. Thus, the surface current densities are reduced to $\boldsymbol{J}_s = \hat{\boldsymbol{n}} \times \boldsymbol{H}_1$ and $\boldsymbol{M}_s = -\hat{\boldsymbol{n}} \times \boldsymbol{E}_1$. Note that $\boldsymbol{J}_s$ (tangential component of $\boldsymbol{H}_1$) and $\boldsymbol{M}_s$ (tangential component of $\boldsymbol{E}_1$) can be measured experimentally or calculated numerically.

2.2. Numerical Implementation of the Surface Equivalence Theorem and Validation for a Single Device

In this paper, the commercial software CST Microwave Studio (CST-MWS) [16] is used to calculate the surface current densities based on the mentioned surface equivalence theorem. To verify the numerical implementation of the surface equivalence theorem, two different types of EMI sources (a dipole antenna and a microstrip patch antenna) are considered, as shown in Figure 2.

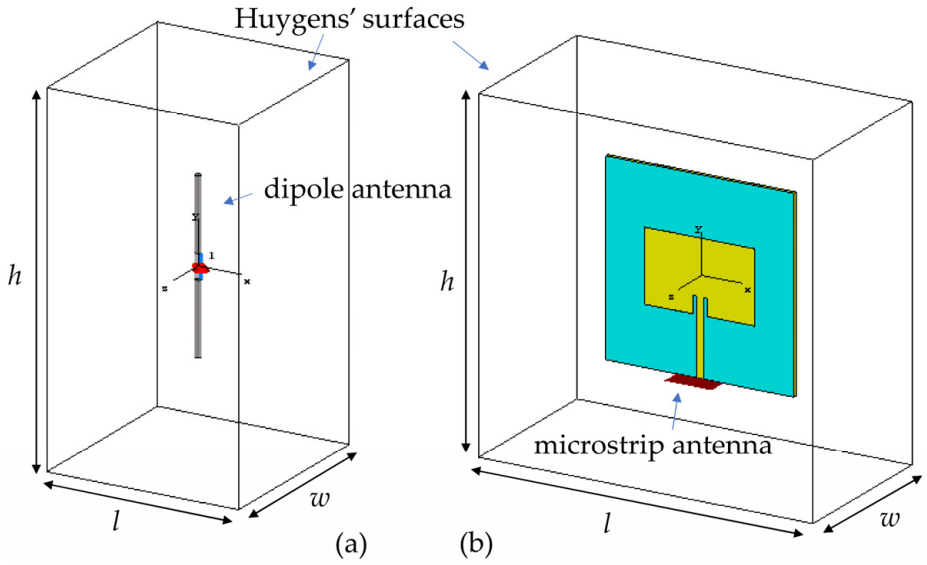

Figure 2. Two different types of EMI sources: (**a**) dipole antenna (thin wire structure) along the *y*-axis, (**b**) microstrip patch antenna.

Figure 2a shows a dipole antenna designed to operate at 1 GHz. The length, radius, and excitation gap of the dipole antenna are 136 mm, 2.5 mm, and 20 mm, respectively. The dipole antenna is enclosed by a Huygens' surface with dimensions $l \times w \times h$, where the center of the dipole antenna coincides with the center of the cuboid, forming the Huygens' surface. The dipole antenna is assumed to be a perfect electric conductor (PEC). A discrete port with a length of 20 mm is used to excite the dipole antenna from its center. To reproduce the results presented in this paper, the CST-MWS input file (dipole_antenna_01.cst) is provided in the Supplementary Materials attached. Figure S1 shows the dipole antenna scattering parameter S_{11} calculated by way of the CST-MWS software using both the time domain finite integration technique (FIT) [17] and the finite element method (FEM) [18].

Figure 2b shows the microstrip antenna, designed to operate at a frequency of 2.4 GHz, inside a cuboid representing the Huygens' surface with dimensions $l \times w \times h$. The center of the front plane of the microstrip antenna coincides with the center of the cuboid (Huygens' surface). The dimensions of the microstrip antenna dielectric are $80 \times 80 \times 1.5$ mm^3. The relative permittivity, permeability, and tangent delta of the microstrip antenna dielectric are 4.08, 1.0, and 0.015, respectively. The dielectric is on the top of a copper plane with a thickness of 0.035 mm. The dimensions of the copper antenna patch are $47 \times 30.2 \times 0.035$ mm^3. The patch antenna is fed by a transmission line with a length of 32.06 mm and a width of 2.98 mm. The transmission line is indented into the patch by 7.16 mm, with a width of 1.5 mm from both sides. To excite the microstrip antenna, a 17.16×10.08 mm^2 waveguide port is used. The CST-MWS file (microstrip_antenna_01.cst) of the microstrip antenna is also provided in the Supplementary Materials attached to this paper. Figure S2 shows the microstrip antenna scattering parameter S_{11} calculated by CST-MWS using both the time domain FIT and the frequency domain FEM. This figure shows that the time domain and frequency domain simulation results are in good agreement with each other.

The radiated electric fields from the dipole antenna at distances of 1 m and 10 m calculated using the integral equation (IE) [19,20] solver in the CST-MWS software are

shown in Figure 3a,b, respectively. To validate the obtained results, the electric fields are also calculated using the equivalent current densities on the Huygens' box of size $150 \times 200 \times 150$ mm^2 using CST-MWS. These results are also depicted in Figure 3. It can be seen that the electric fields obtained by the equivalent current densities on the Huygens' surface are in very good agreement with those of the source directly calculated using the IE full-wave solver. The maximum absolute difference in Figure 3 is 0.15 dB. The same procedure is repeated for a distance of 3 m between the observation point and the dipole antenna, and the results are shown in Figure S3. It should be noted that the radiated electric field for the dipole antenna (shown in Figure 2a) decreases by about $20 \times \log10(R_1/R_2) = -20$ dB when the distance to the observation point increases from $R_1 = 1$ m to $R_2 = 10$ m.

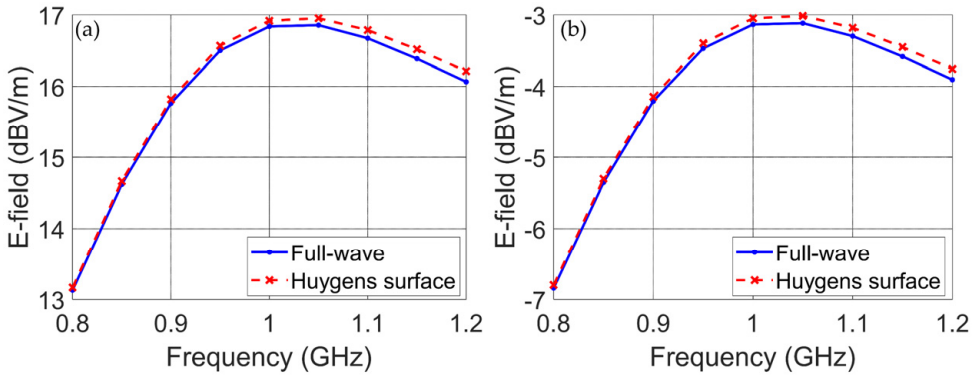

Figure 3. The radiated electric field of the dipole antenna shown in Figure 2a: (**a**) at a distance of 1 m along the *z*-axis from the center of the dipole antenna, (**b**) at a distance of 10 m along the *z*-axis from the center of the dipole antenna.

The radiated electric fields in two two-dimensional (2D) cut planes, $\varphi = 0$ (*xoz* plane) and $\theta = 90$ (*xoy* plane), according to Figure 2a, are shown in Figure 4a,b. It can be seen that the results obtained by the equivalent Huygens' surface method are in excellent agreement with the results obtained using the full-wave IE solver.

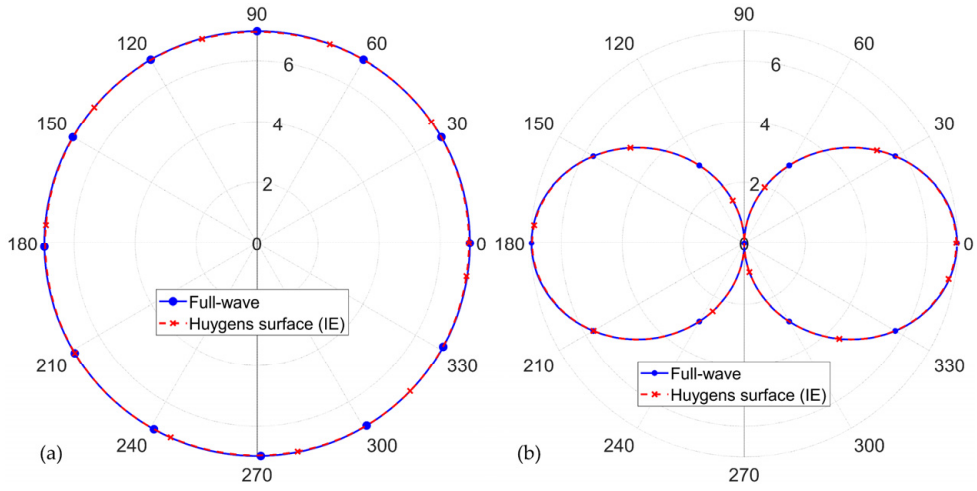

Figure 4. The 2D cut planes of the radiated electric field: (**a**) at $\varphi = 0$ or *xoz* plane, (**b**) at $\theta = 90$ or *xoy* plane.

The same procedure using a Huygens' box of $105 \times 150 \times 100$ mm^3 was repeated for the microstrip antenna shown in Figure 2b. Figure 5a,b show the radiated electric fields at distances of 1 m and 10 m from the top face of the microstrip antenna along the *z*-axis. The direct results obtained using the full-wave method are shown by a dashed red line with cross (×) markers, while the results obtained using the equivalent sources

on the Huygens' surface are shown by dashed blue lines. It should be noted that the radiated electric field for the microstrip antenna (shown in Figure 2b) decreases by about $20 \times \log10(R_1/R_2) = -20$ dB when the distance to the observation point increases from $R_1 = 1$ m to $R_2 = 10$ m.

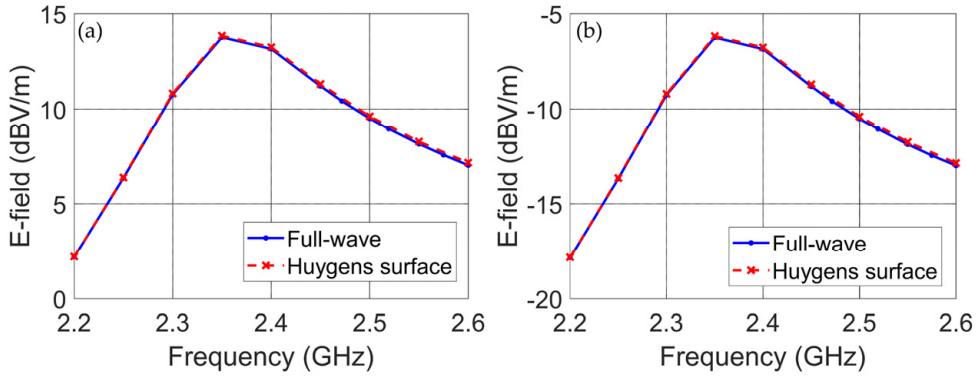

Figure 5. The radiated electric field of the microstrip antenna shown in Figure 2b: (**a**) at a distance of 1 m along the z-axis from the top of the antenna, (**b**) at a distance of 10 m along the z-axis from the top of the antenna.

To evaluate the performance of the equivalent Huygens' surface, 2D cut planes at $\varphi = 0$ and $\theta = 90$ at 10 m distance are shown in Figure 6a,b, respectively. The maximum absolute difference between the calculated electric field using the full-wave method and the equivalent Huygens' surface method is -26.02 dB (0.05 V/m) and -27.97 dB (0.04 V/m) in the $\varphi = 0$ and $\theta = 90$ cut planes, respectively.

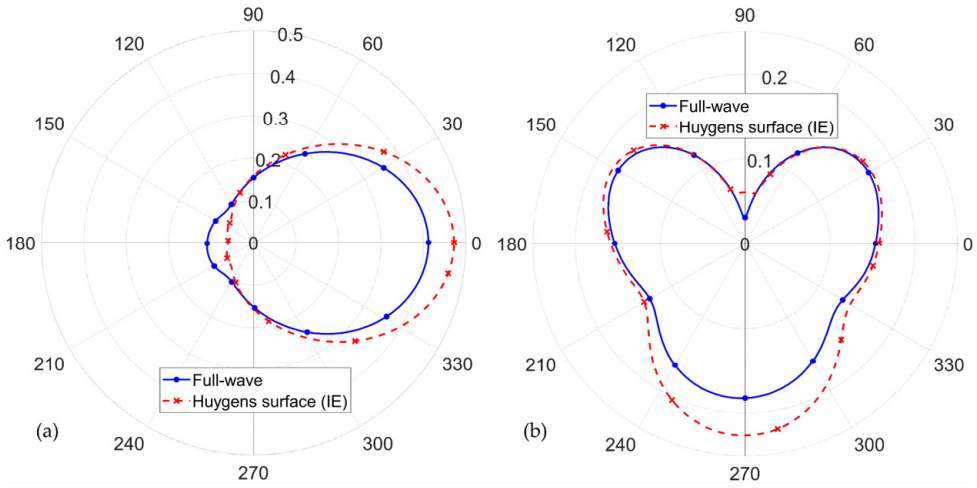

Figure 6. The 2D cut planes of the radiated electric field: (**a**) at $\varphi = 0$ or xoz plane, (**b**) at $\theta = 90$ or xoy plane.

The above examples show that the implementation of the surface equivalence theorem using the CST-MWS software provides enough accuracy to calculate the radiated emissions from a single EMI source.

To show the impact of the Huygens' box size on the calculated results, three different boxes with dimensions of $20 \times 200 \times 20$ mm^3, $70 \times 200 \times 70$ mm^3, and $150 \times 200 \times 150$ mm^3 are considered. Figure 7 shows the radiated emissions for these three box sizes. Although the Huygens' box cross-section increases approximately by a factor 4 in each case, the radiated electric field does not change significantly.

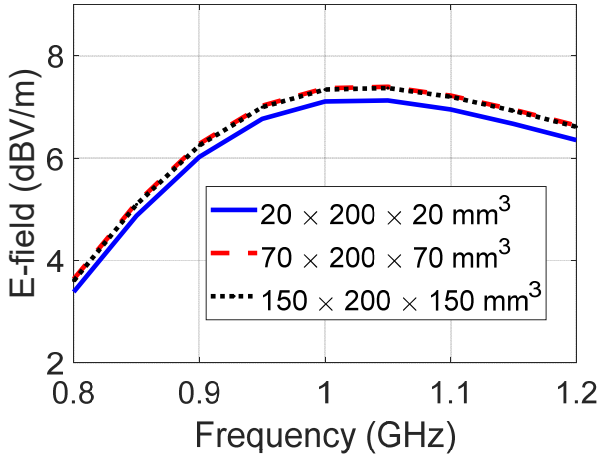

Figure 7. Radiated emission obtained considering three different Huygens' box sizes: $20 \times 200 \times 20$ mm^3 (solid blue line), $70 \times 200 \times 70$ mm^3 (dashed red line), and $150 \times 200 \times 150$ mm^3 (dotted black line).

2.3. Calculation of Radiated Emission from Multiple EMI Sources Using the Surface Equivalence Theorem

Here, the radiated emissions from multiple EMI sources are calculated using the surface equivalence theorem. To achieve this, the equivalent electric densities calculated around the Huygens' surfaces for each element are used. The location and orientation of each EMI source can be determined using six independent parameters, three for the position and three for the orientation. Without loss of generality, consider the microstrip shown in Figure 2b as an EMI source. This EMI source can be located at an arbitrary point in space defined by (x_i, y_i, z_i), where x_i, y_i, and z_i are the distances between the origin and the center of the EMI source along the x-, y-, and z-axis, respectively. The orientation of the ith EMI source is defined by $(\alpha_i, \beta_i, \gamma_i)$, where α_i, β_i, and γ_i are the rotation angels of the EMI source around the x-, y-, and z-axis, respectively.

For example, Figure 8 shows an arrangement for three microstrip antennas. The location vector (x_i, y_i, z_i) and orientation vector $(\alpha_i, \beta_i, \gamma_i)$ for each microstrip antenna are also shown in this figure. This example illustrates that by changing the position and orientation vectors, any configuration involving multiple devices can be easily constructed. Note that the number of EMI sources and their location and orientation vectors can be selected arbitrarily without any limitation.

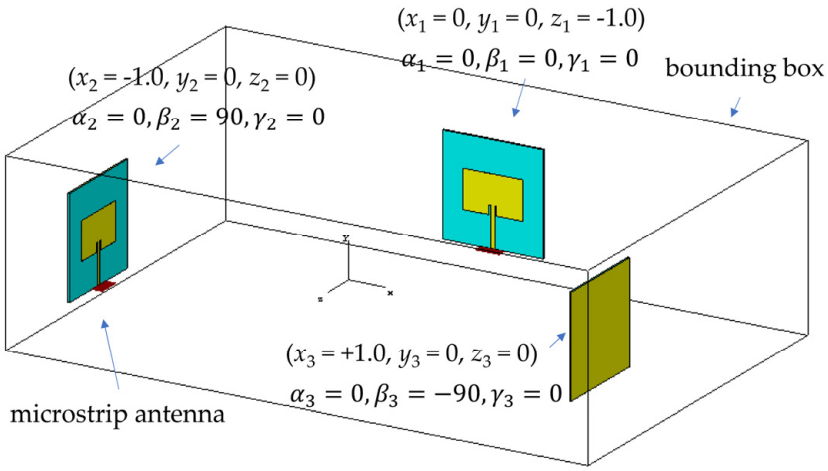

Figure 8. An example of the presence of three EMI sources (microstrip antennas) with different location and orientation vectors.

To verify the results of using the equivalent current densities on the Huygens' surfaces for multiple devices, the considered geometry in Figure 8 is simulated using the full-wave IE solver, and the radiated electric field at the origin (0, 0, 0) is calculated. The radiated y-component of the electric field (vertical component) calculated by the full-wave IE solver is shown in Figure 9 by a solid blue line. The y-component of the electric field radiated by a single microstrip antenna multiplied by 3 is also shown by a dash–dot black line in this figure. Since the geometry is selected so that the observation point at the origin detects the same structure for each device, the radiated y-component of the electric field from a single microstrip antenna can be multiplied by 3 and used for all the elements. Finally, the radiated y-component of the electric field obtained using the equivalent current densities on the Huygens' surface is also presented in Figure 9 in dashed red lines. Two values for the distance between the observation point and each EMI source are considered (1 m and 3 m), and the results are presented in Figure 9a,b, respectively. The differences between the full-wave approach and the equivalent method in Figure 9a is due to the effects of coupling between the elements. When the distance between the elements is increased threefold (see Figure 9b), the coupling is decreased and the agreement improves. This example shows that the equivalent current densities on the Huygens' surface cannot be used for closely spaced multiple devices.

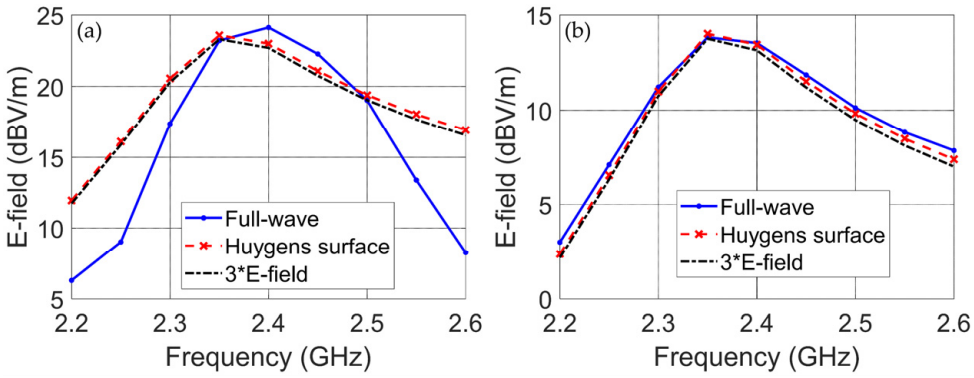

Figure 9. The radiated electric field of the three microstrip antennas shown in Figure 8: (**a**) the distances between the EMI sources and the observation point are 1 m, (**b**) the distances between the EMI sources and the observation point are 3 m.

Using Huygens' surface allows a significant reduction in the computation time and memory resources. For example, in this case study, to obtain the results shown in Figure 9b, in which the distance between the observation point and each EMI source is 3 m, the 23,882,040 mesh cells required in the time domain FIT solver make it impossible to simulate on a simple laptop with 32-gigabyte random access memory (RAM). Meanwhile, the Huygens' surface method only needs 520 mesh cells to model each EMI source. In the Supplementary Materials (Figure S4), it is shown that the interaction between the elements becomes negligible even at a distance of 1.5 m between the observation point (at the origin) and EMI sources. Figure S5a,b show the electric field calculated at other observation points, namely (0.5, 0, 0) and (−0.5, 0, 0).

The same configuration as the one shown in Figure 8 is repeated considering, as a source, the dipole antenna shown in Figure 2a. In this example, the location vectors for the dipole antennas are the same as in the previous example (i.e., $x_1 = 0$, $y_1 = 0$, $z_1 = -1.0$ m for the first dipole; $x_2 = -1.0$ m, $y_2 = 0$, $z_2 = 0$ for the second dipole; and $x_3 = 1.0$ m, $y_3 = 0$, $z_3 = 0$ for the last dipole) with an orientation vector ($\alpha_i = 0$, $\beta_i = 0$, $\gamma_i = 0$), where $i = 1, 2, 3$. The radiated electric field calculated for the three dipole antennas at distances of 1 m and 3 m are shown in Figure 10. It should be noted that the dipole antennas are located on a circle with a radius of either 1 m or 3 m around the origin. It can be seen that by increasing the distance between the EMI sources (or increasing the radius of the circle on which the EMI sources are located), the interaction between them is reduced and

the agreement between the equivalent method and the full-wave approach is improved. Figure S6 in the Supplementary Materials shows the radiated electric field for the case where the distance between the observation point and each EMI source (dipole antenna) is 10 m. To calculate the results shown in Figure S6 (10 m distance) using the time domain FIT solver, 115,240,320 mesh cells are needed, while each EMI source is modeled using only 35 mesh cells in the equivalent Huygens' surface method.

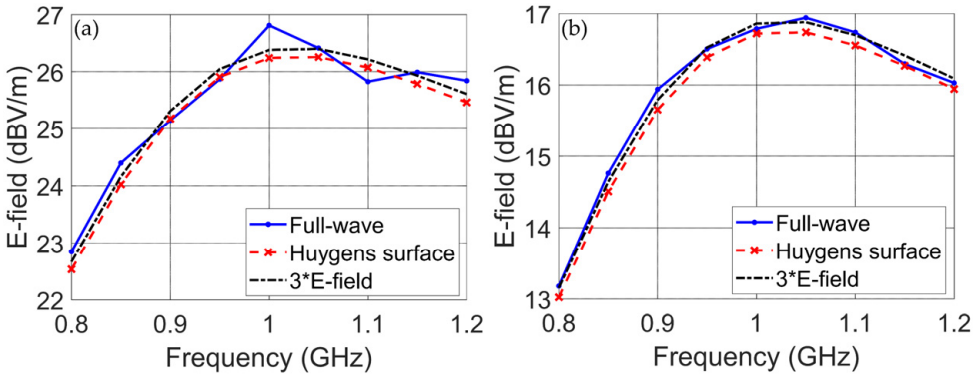

Figure 10. The radiated electric field of three dipole antennas in the same configuration as in Figure 8: (**a**) the distance between the EMI sources and the observation point is 1 m, (**b**) the distance between the EMI sources and the observation point is 3 m.

3. Application of the Method to Calculate the Radiated Emissions from Multiple Devices

Here, the surface equivalence theorem presented in the previous section is used to calculate the radiated emissions from multiple EMI sources. To achieve this, three different configurations for the EMI sources are considered, which will be presented in the next subsection. Using the surface equivalence theorem, the equivalent electric and magnetic current densities are calculated on a box enclosing each EMI source for different scenarios. Then, these equivalent current densities are used to calculate the radiation emissions from all of the EMI sources.

3.1. The Considered Configurations of EMI Sources

This subsection describes the three different configurations considered in the paper.

3.1.1. One-Dimensional Linear Array of EMI Sources

In the first configuration, the EMI sources (here considered to be dipole antennas) are placed in a linear array (similar to the configuration in [5]) parallel to the x-axis located at $z = d$, as shown in Figure 11. The distance between two successive elements is sx. The orientation of each element can be selected arbitrarily by choosing the rotation angles around the x-, y-, and z-axes. The radiated emission from the multiple EMI sources placed in a one-dimensional linear array is calculated at an observation point (OP) located at the center of the coordinate system, as shown in Figure 11.

3.1.2. Two-Dimensional Rectangular Array of EMI Sources

In the second configuration, the EMI sources are placed in a rectangular array parallel to the xoy plane at $z = d$ (similar to the configuration in [6]), as shown in Figure 12. The distances between two successive elements in the x and y directions are defined by sx and sy, respectively. The orientation of each element in the array can be selected arbitrarily by choosing the rotation angles around the x-, y-, and z-axes. The radiated emissions from the multiple EMI sources placed in a two-dimensional rectangular array are calculated at an OP in the center of the coordinate system, as shown in Figure 12.

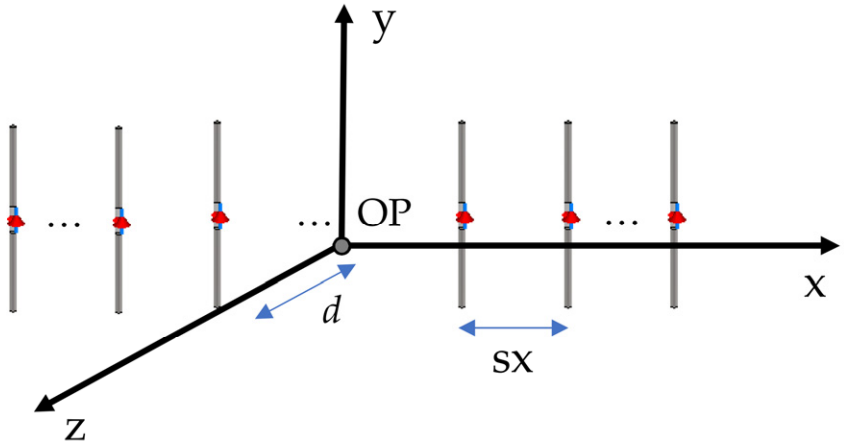

Figure 11. A linear, equally spaced array of EMI sources along the *x*-axis with an arbitrary number of radiation elements.

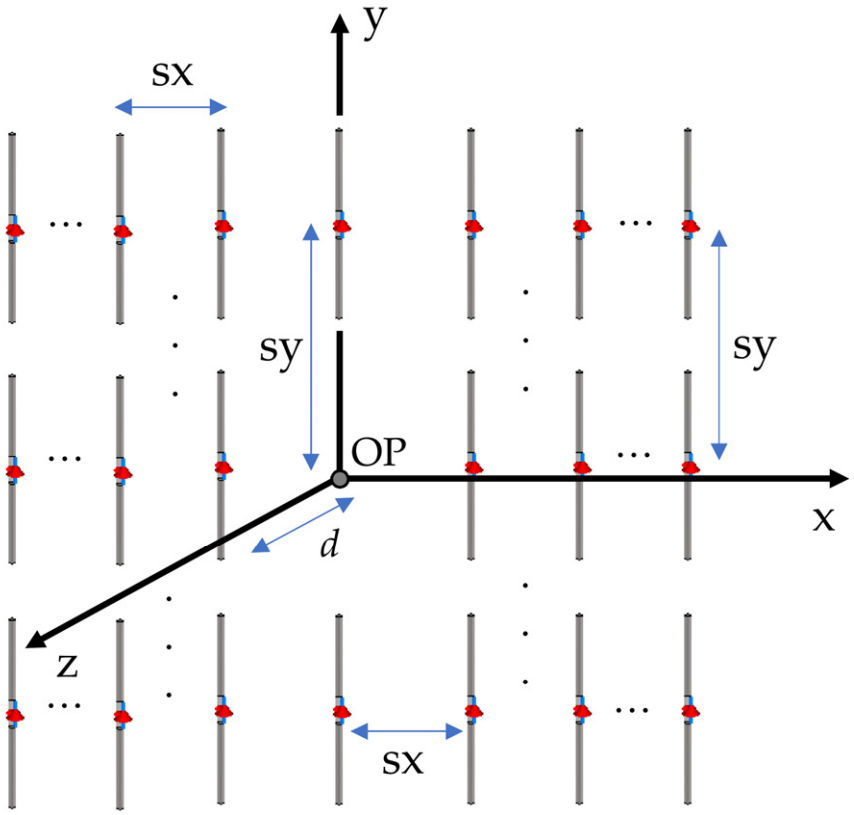

Figure 12. A rectangular two-dimensional array of EMI sources parallel to the *xoy* plane with an arbitrary number of radiation elements.

3.1.3. Three-Dimensional Array of EMI Sources

In the third configuration, the EMI sources are placed in a three-dimensional distribution (similar to the configuration in [6]), as shown in Figure 13. The distances between two successive elements in the *x*, *y*, and *z* directions are defined by sx, sy, and sz, respectively. The orientation of each element in the array can be selected arbitrarily by choosing the rotation angles around the *x*-, *y*-, and *z*-axes. The radiated emissions from the multiple EMI sources placed in a three-dimensional array are calculated at the OP, located at the center of the coordinate system, as shown in Figure 13. Note that in the three-dimensional distribution array, the first plane including sources is located at $z = d$.

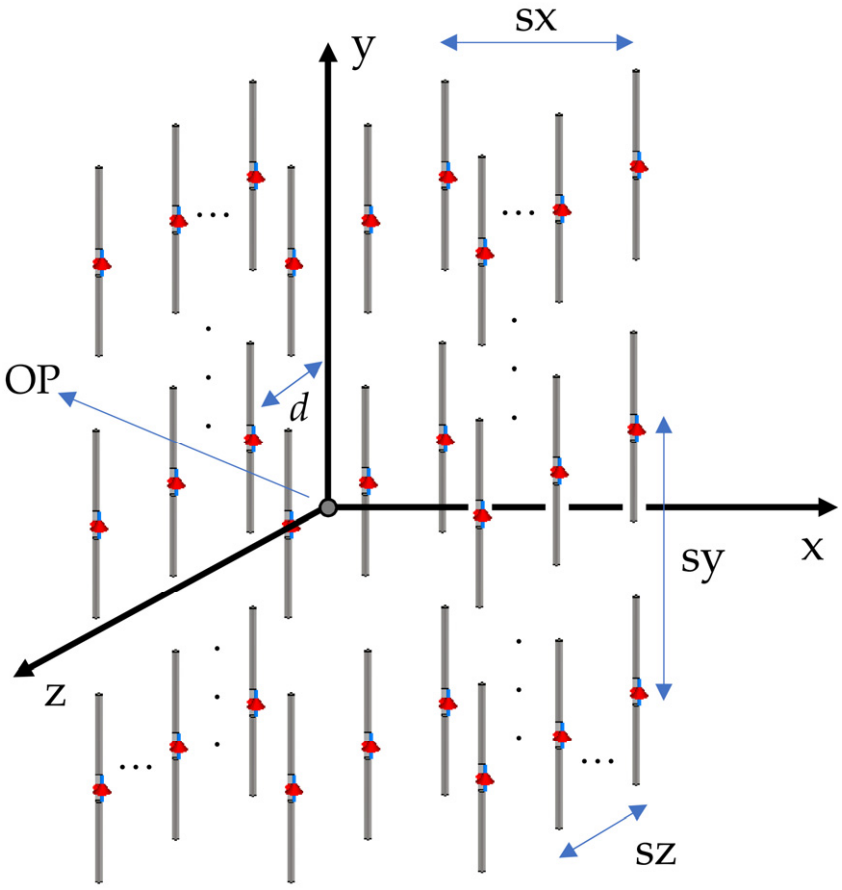

Figure 13. A three-dimensional array of EMI sources in free space with an arbitrary number of radiation elements.

3.2. Radiation from Multiple EMI Sources Configured in a One-Dimensional Linear Array

In this case study, the dipole antenna shown in Figure 2a is considered as the EMI source element. The distance sx between two adjacent elements is 1 m. In this example, three cases involving correlated elements (same phase), uncorrelated elements (random phase), and uncorrelated elements with random orientation are examined. Figure 11 shows the one-dimensional configuration with the same orientation for all the EMI sources. Different numbers of devices (1, 3, 5, 7, and 9) were considered in this case study.

The simulated results for this case study are summarized in Table 2. The first column of Table 2 shows the calculated in-phase radiated field for 1, 3, 5, 7, and 9 correlated elements at 1 GHz.

Table 2. The radiated emission at a minimum distance of 3 m from the devices. The radiated emissions for the correlated case study are provided for comparison purposes in the first column.

	Radiated Emissions for Correlated Devices (V/m)	Mean and Std of the Radiated Emissions for Uncorrelated Devices (V/m)	Mean and Std of the Radiated Emissions for Uncorrelated Devices with Random Orientation (V/m)
Single EUT	2.28	—	—
3 devices	2.19	Mean: 3.35 Std: 1.52	Mean: 2.26 Std: 1.14
5 devices	1.96	Mean: 4.11 Std: 2.07	Mean: 2.77 Std: 1.43
7 devices	4.26	Mean: 4.56 Std: 2.26	Mean: 3.02 Std: 1.60
9 devices	2.59	Mean: 4.90 Std: 2.47	Mean: 3.30 Std: 1.73

According to the first column of Table 2, the radiated emissions at a distance of 3 m for a single dipole antenna at 1 GHz is 2.28 V/m. Increasing the number of devices to three and five does not lead to an increase in the total in-phase radiated emissions. For example, for three devices, the radiated emission level is 2.19 V/m, which is lower than the emissions associated with a single piece of equipment under test (EUT). This result is opposite to the results presented by Haberlin [6]. In [6], increasing the number of radiative elements increases the radiated emissions. This is because the actual pattern of the dipole antenna is considered in our work with its phase varied by the term exp(-*jkR*), where *j*, *k*, and *R* are the complex imaginary number, the wavenumber, and the distance, respectively. This means that the different distances to the observation point from each device can lead to different phases, and therefore, to constructive or destructive interference, thus changing the level of the overall radiated emission. This shows how the radiation pattern and the location of the considered devices affect the far-field radiated emission.

To better illustrate this effect, the first column of Table 2 is plotted in Figure 14. In this figure, the far-field radiated emission for the assumed linear configuration (as shown in Figure 11) is plotted as well. It can be seen that the actual radiated emission from multiple devices can be different from the power sum formula presented in [5,6].

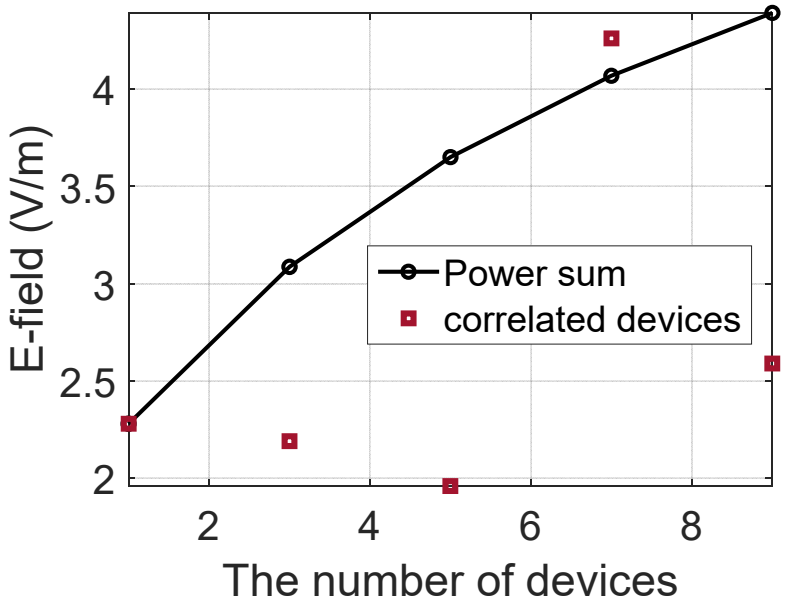

Figure 14. The radiated emission from multiple devices. The solid black line and red squares represent the power sum formula and the emissions from correlated devices, respectively.

The second column of Table 2 presents the statistical values (mean value and standard deviation) obtained from Monte Carlo simulations [21,22] with 1000 samples with random phases. It can be seen that both the mean value and the standard deviation increased when the number of devices increases from one to nine elements. Figure 15a,b show the mean value and standard deviation of the radiated emissions for three and nine uncorrelated devices, respectively, in the frequency range from 0.8 to 1.2 GHz. In these figures, the central black lines are the mean values and the upper and lower red dashed lines show the mean value plus and minus one standard deviation. Figure S7a,b show the radiated emissions for three and nine uncorrelated devices, respectively, in the frequency range from 0.8 to 1.2 GHz for 1000 Monte Carlo simulations.

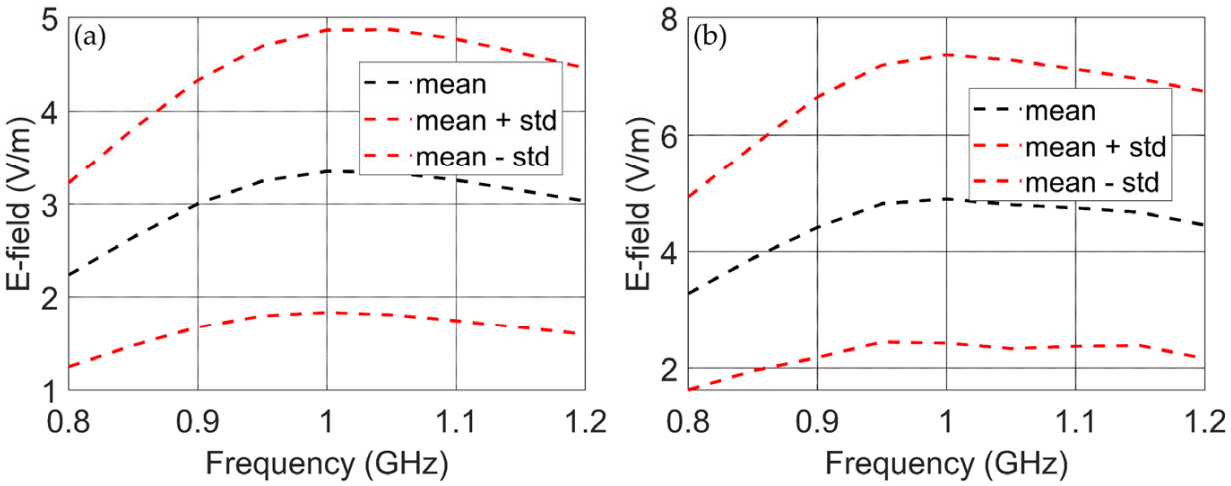

Figure 15. The radiated emission from multiple devices with random phase in the frequency range from 0.8 to 1.2 GHz: (**a**) for three devices, (**b**) for nine devices. The black dashed line and the red dashed lines are the mean value and the mean value plus and minus one standard deviation, respectively.

The third column of Table 2 presents the statistical values (mean value and standard deviation) obtained from Monte Carlo simulations with 1000 samples with random phases and orientations. For simplicity, the devices were only rotated around the *x*-axis with reference to the configuration shown in Figure 11. The results presented in the third column show that the level of radiated emissions will increase when the number of devices increases. It should be noted that the level of increase is lower than in the second column, in which the random orientation of the devices is not considered. Figure S8a,b show the radiated emissions for three and nine uncorrelated devices with random orientation, respectively, in the frequency range from 0.8 to 1.2 GHz for 1000 Monte Carlo simulations.

The simulated results for a linear array of multiple EMI sources with frequencies of 0.8, 0.9, 1.1, and 1.2 GHz are summarized in Tables S1–S4, respectively. The first column of these tables shows the calculated in-phase radiated field for 1, 3, 5, 7, and 9 correlated elements. The second column of Table S1 to S4 presents the statistical values (mean value and standard deviation) obtained from Monte Carlo simulations with 1000 samples with random phases. Finally, the third column of Table S1 to S4 presents the statistical values (mean value and standard deviation) obtained from Monte Carlo simulations with 1000 samples with random phases and orientations.

Tables S1–S4 show that the increasing the number of EMI sources lead to an increase in the radiated emission regardless of the frequency of the EMI sources.

To investigate the effect of the separation distances between elements in the uniform linear configuration shown in Figure 11., the radiated electric field for three different case studies (sx = 2 m, 4 m, and 6 m) using Monte Carlo simulation is presented in Figure 16. As can be seen, despite the fact that increasing the distance sx between the source elements will decrease the radiated emission, the trend of the mean values remains ascending when the number of elements increases. Note that the minimum distance between the radiator elements and the OP is 3 m.

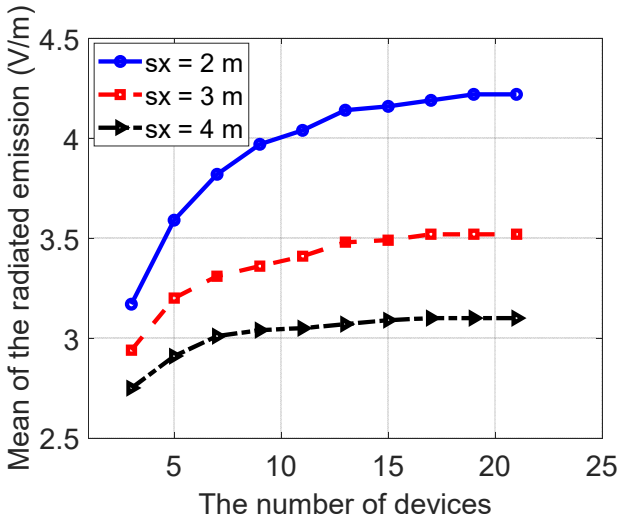

Figure 16. The mean of the radiated emission from multiple radiator elements with different separation distances: sx = 2 m (blue line), sx = 3 m (red dashed line), and sx = 4 m (black dashed line).

A nonuniform linear array with randomly selected separation distances between the elements is also investigated. In this configuration, the following assumptions according to Figure 11 are considered: (1) the radiating elements are located between $x_{\min} = -(N-1) \times sx_{\min}$ and $x_{\max} = +(N-1) \times sx_{\min}$, where N is the number of elements and $sx_{\min}$ is the minimum distance between the elements; (2) the OP is located at ($x = 0$, $y = 0$, $z = 10$ m). Here, the minimum distance between the radiator elements and OP is 10 m.

Figure 17 shows the mean values of the radiated emissions for nonuniform linear ar-rays. It can be seen that as the number of radiating elements increases, the mean value of the total radiation of the array increases regardless of the minimum separation distances between the elements.

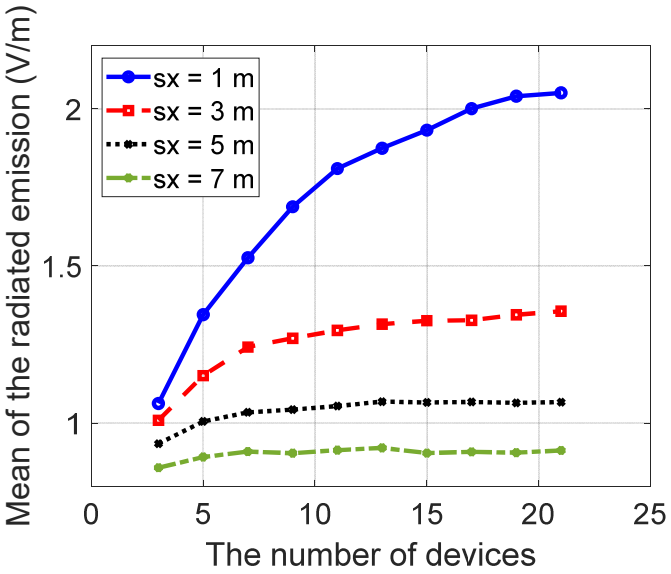

Figure 17. The mean of the radiated emission from multiple radiator elements with nonuniform separation distances. The blue line, red dashed line, black dotted line, and green dash–dot lines are the results for minimum separation distances (sx-min) of 1 m, 3 m, 5 m, and 7 m, respectively.

3.3. Radiation from Multiple EMI Sources Configured in a Two-Dimensional Linear Array

Similar to the previous example, the dipole antenna shown in Figure 2a is considered as the EMI source element. In this example, three cases involving correlated, uncorrelated, and uncorrelated with random orientation of the devices are also examined. Figure 12

shows the two-dimensional configuration with the same orientation for all the EMI sources. The vertical and horizontal distances sy and sx between adjacent elements of this two-dimensional array are 1 m. Different numbers of devices (1, 9, 25, 49, and 81) are considered in this case study.

The simulated results for this case study are presented in Table 3. The first column of Table 3 shows the calculated in-phase radiated field for 1, 9, 25, 49, and 81 correlated elements at 1 GHz. The second column of the table presents the statistical values (mean value and standard deviation) obtained from Monte Carlo simulations with 1000 samples with random phases. The third column of Table 3 presents the statistical values (mean value and standard deviation) obtained from Monte Carlo simulations with 1000 samples with random phases and orientations. For simplicity, the devices are only rotated around the *x*-axis with reference to Figure 12.

Table 3. The radiated emission at a minimum distance of 3 m from the EUT. The radiated emissions for the correlated case study are provided for comparison purposes in the first column.

	Radiated Emissions for Correlated Devices (V/m)	Mean and Std of the Radiated Emissions for Uncorrelated Devices (V/m)	Mean and Std of the Radiated Emissions for Uncorrelated Devices with Random Orientation (V/m)
Single EUT	2.28	—	—
3 × 3 devices	1.39	Mean: 5.21 Std: 2.58	Mean: 3.66 Std: 1.88
5 × 5 devices	4.39	Mean: 7.41 Std: 3.76	Mean: 5.43 Std: 2.90
7 × 7 devices	4.26	Mean: 8.89 Std: 4.63	Mean: 6.32 Std: 3.44
9 × 9 devices	12.13	Mean: 9.55 Std: 5.01	— —

According to the first column of Table 3, the radiated emission at a distance of 3 m for a single dipole antenna at 1 GHz is 2.28 V/m. Increasing the number of devices to nine (3 × 3), the in-phase radiated emission decreased to 1.39 V/m. The reason for this decrease was explained in detail in the previous subsection. In this case, the radiated emission obtained by the power sum formula is about 6.40 V/m, which is greater than the in-phase radiation emission. It is worth noting that this case study contradicts previous works such as [6], in which increasing the number of interference sources was shown to lead to an increase in the radiated emission. However, the first column of Table 3 shows that the number of elements alone cannot account for the total radiation emission. As expected, for all cases (3 × 3, 5 × 5, 7 × 7, and 9 × 9 devices), the mean values for the uncorrelated devices with random orientation (column 3 in the table) are lower than those in which all the devices have the same orientation (column 2 in the table). This illustrates the importance of considering the effects of the orientation of radiating elements to the total radiation.

The second and third columns of Table 3 show that increasing the number of interference sources leads to an increase in the mean and standard deviation of the radiated emissions of uncorrelated devices, regardless of whether or not their orientations are considered.

Figure 18a,b show the mean and standard deviation of the radiated emissions for uncorrelated 3 × 3 and 9 × 9 devices in the frequency range from 0.8 to 1.2 GHz, respectively. In these figures, the central black lines are the mean values and the upper and lower dashed red lines show the mean value plus and minus one standard deviation, respectively. Figure S9a,b show the radiated emissions for 3 × 3 and 9 × 9 uncorrelated devices, respectively, in the frequency range from 0.8 to 1.2 GHz for 1000 Monte Carlo simulations. Figure S10a,b also show the radiated emissions for 3 × 3 and 7 × 7 uncorrelated devices with random orientations, respectively, in the frequency range from 0.8 to 1.2 GHz for 1000 Monte Carlo simulations.

The simulated results for a two-dimensional linear array of multiple EMI sources with frequencies of 0.8, 0.9, 1.1, and 1.2 GHz are summarized in Tables S5–S8, respectively. The first column of these tables shows the calculated in-phase radiated field for 3 × 3, 5 × 5, 7 × 7, and 9 × 9 correlated elements. The second column of Tables S5–S8 provides the statistical values (mean value and standard deviation) obtained from Monte Carlo simulations with 1000 samples with random phases. Finally, the third column of Tables S5–S8 presents the statistical values (mean value and standard deviation) obtained from Monte Carlo simulations with 1000 samples with random phases and orientations.

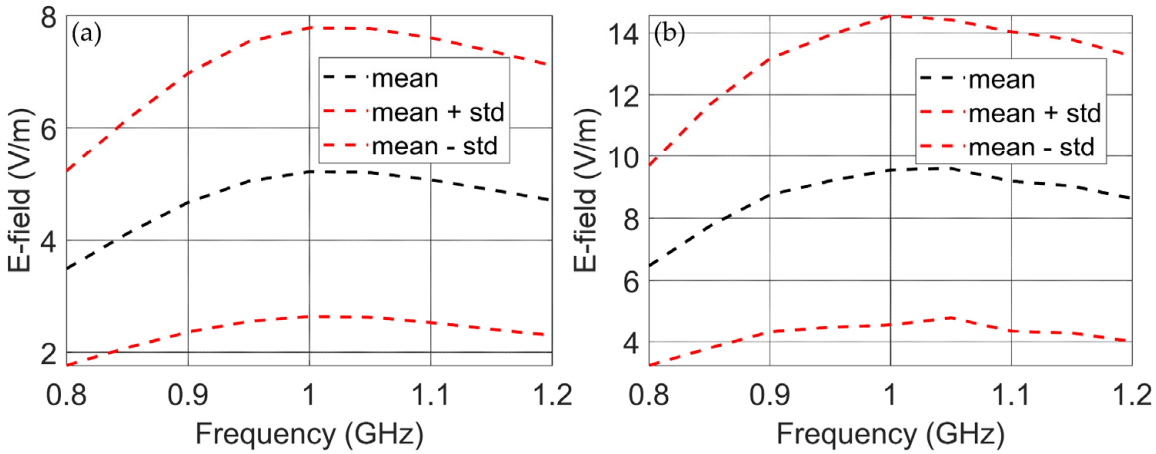

Figure 18. The radiated emission from multiple devices with random phase in the frequency range from 0.8 to 1.2 GHz: (**a**) for 3 × 3 devices, (**b**) for 9 × 9 devices. The black dashed lines represent the mean value and the red dashed lines represent the mean value plus and minus one standard deviation.

Tables S5–S8 show that the increasing the number of EMI sources lead to an increase in the radiated emission regardless of the frequency of the EMI sources.

Similar to the one-dimensional linear array, the obtained results show that, in general, increasing the number of devices will increase the radiated emissions; this is as expected, and in agreement with previous studies [5–8].

3.4. Radiation from Multiple EMI Sources Configured in a Three-Dimensional Linear Array

In the three-dimensional case study, the dipole antenna shown in Figure 2a is also considered as the EMI source element. In this example, three cases involving correlated, uncorrelated, and uncorrelated devices with random orientation are examined. Figure 13 shows the three-dimensional configuration with the same orientation for all the EMI sources. Different numbers of devices (9, 18, 17, 25, and 50) are considered in this case study.

The simulated results for this case study are presented in Table 4. The second column of Table 4 shows the calculated in-phase radiated field for 9, 18, 17, 25, and 50 correlated elements at 1 GHz. The third column of the table provides the statistical values (mean value and standard deviation) obtained from Monte Carlo simulations with 1000 samples with random phases. The fourth column of Table 4 presents the statistical values (mean value and standard deviation) obtained from Monte Carlo simulations with 1000 samples with random phases and orientations. For simplicity, the devices are only rotated around the *x*-axis.

According to the second column of Table 4, the radiated emission at a distance of 3 m for a single dipole antenna at 1 GHz is 2.28 V/m. The same trends as in the 1D and 2D cases can also be observed here.

Table 4. The radiated emission at 3 m from the EUT. The radiated emissions for the correlated case study are provided for comparison purposes in the first column.

	Radiated Emissions for Correlated Devices (V/m)	Mean and Std of the Radiated Emissions for Uncorrelated Devices (V/m)	Mean and Std of the Radiated Emissions for Uncorrelated Devices with Random Orientation (V/m)
Single EUT	2.28	—	—
$3 \times 3 \times 1$ devices	1.39	Mean: 5.21 Std: 2.58	Mean: 3.66 Std: 1.88
$3 \times 3 \times 2$ devices	3.98	Mean: 6.84 Std: 3.58	Mean: 4.65 Std: 2.46
$5 \times 5 \times 1$ devices	4.39	Mean: 7.41 Std: 3.76	Mean: 5.43 Std: 2.90
$5 \times 5 \times 2$ devices	9.34	Mean: 9.62 Std: 5.03	Mean: 6.72 Std: 3.58

3.5. Radiation from Multiple Uncorrelated Devices with Arbitrary Locations and Orientations

In this case study, multiple uncorrelated devices with arbitrary locations and orientations are considered. The microstrip antenna shown in Figure 2b is used in this case study. Two devices are assumed to be located inside a cubic volume of 1 m^3. The locations and orientations of both devices are randomly selected inside that volume. Figure 19a shows, as an example, the radiated emission patterns from the two devices inside the room when both devices are located at different positions and have different orientations. The considered locations and orientations of the devices are shown in Figure 19a by the blue cubes.

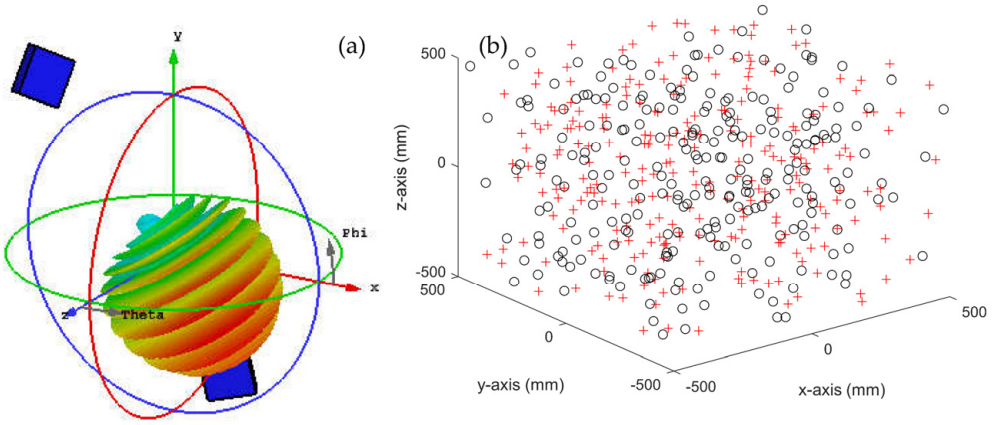

Figure 19. (**a**) The radiated emission patterns of two devices with different locations and orientations. (**b**) The randomly assumed locations of the two devices inside the cubical volume. Red pluses and black circles show the arbitrary locations.

To carry out a statistical analysis of the effect of the locations and orientations of the devices, a Monte Carlo simulation was performed. The red pluses and black circles in Figure 19b show the arbitrary locations for each of the devices. The observation point is located 10 m away from the center of the cube.

After the Monte Carlo simulations, the mean and standard deviation of the obtained results were calculated. Figure 20 shows the radiated emissions in the planes $\varphi = 90^{\circ}$ and $\theta = 90^{\circ}$. For comparison, the radiated emissions from a single EUT are also shown in this figure. The blue curves show the mean value and the red dashed curves show the mean value plus and minus the standard deviation.

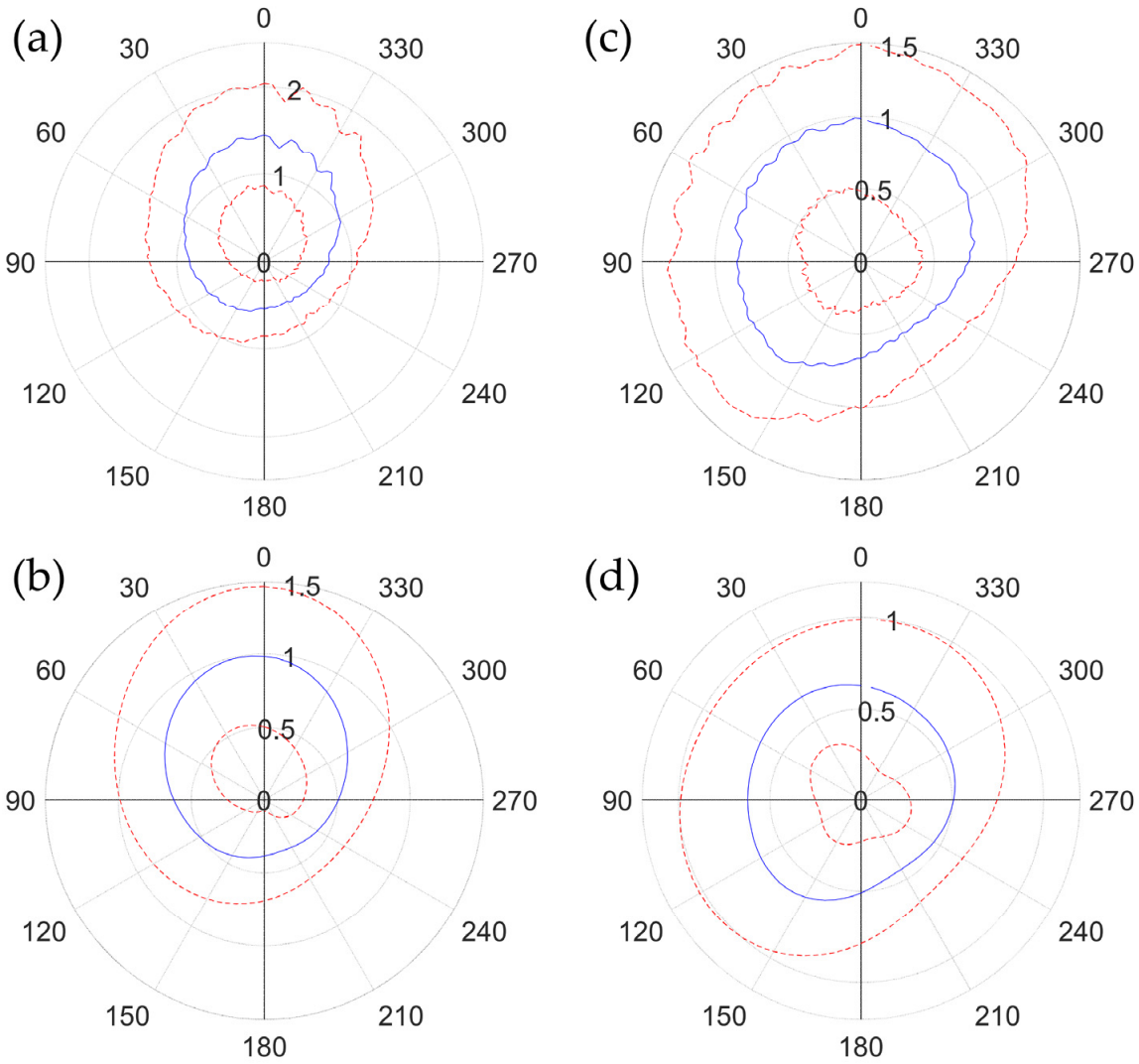

Figure 20. The radiated emission (in V/m) in plane $\varphi = 90^{\circ}$ (**a**) from two uncorrelated microstrip antennas and (**b**) from one microstrip antenna. The radiated emission (in V/m) in plane $\theta = 90^{\circ}$ (**c**) from two uncorrelated microstrip antennas and (**d**) from one microstrip antenna. Blue curves show the mean value and the red dashed curves show the mean value plus and minus the standard deviation.

It can be seen from Figure 20a,b that doubling the number of devices leads to slightly higher radiated emissions (by about 0.5 V/m). Note that the maximum radiated emission (considered here as the sum of the mean value and one standard deviation) from a single microstrip antenna is 1.4 V/m. However, if the orientation of the devices is selected randomly, the mean value of the radiated emission reduces to about 1 V/m. This confirms that the orientations of the EUT(s) are important in calculating the mean radiation.

It can be seen from Figure 20c,d that increasing the number of devices also leads to higher radiated emissions in the $\theta = 90^{\circ}$ plane. As in Figure 20a,b, the blue curves in Figure 20c,d show the mean value and the red dashed curves show the mean value plus and minus the standard deviation. By increasing the number of devices from 1 to 2, the mean value is increased by 0.5 V/m when the locations and orientations of both devices are selected randomly.

4. Discussion and Conclusions

The surface equivalence theorem was used to obtain the far-field radiation from multiple devices with arbitrary orientations and locations. To achieve this, the near-

field electric and magnetic fields were calculated in six different planes around each EUT (Huygens' surface). These calculations were used to estimate the far-field radiation from multiple devices with arbitrary orientations and locations. The proposed method was validated using full-wave simulations.

In the carried out investigations, three cases were considered:

- Radiation from multiple correlated devices;
- Radiation from multiple uncorrelated devices;
- Radiation from multiple uncorrelated devices with arbitrary locations and orientations.

In general, the radiated emissions can be estimated by multiplying the radiated emissions of single elements by an array factor including the phase effects. The proposed method was used to validate previous works presented in the literature.

When the multiple devices have random phases, the radiated emissions can be estimated using the power sum formula. Here, it should be noted that the power sum formula is valid only for one orientation and location of the devices. If the locations and orientations of the devices are randomly selected (consistent with more realistic conditions), the power sum formula presented by previous investigations fails. In this paper, Huygens' surface was used to represent each EUT, and Monte Carlo simulations were performed considering the arbitrary locations and orientation of the devices to evaluate radiated emissions from multiple devices. The proposed approach using Huygens' surfaces allows one to consider arbitrary patterns for each device. Furthermore, the Monte Carlo simulations help to model random locations and orientations for each EUT.

The obtained results show that, in general, increasing the number of devices will increase the radiated emissions, as expected and in agreement with previous studies. Furthermore, it can be seen that considering the more realistic condition of random locations and orientations, the increase in the radiated emissions will be lower than the predictions of previous studies, which use the power sum formula.

Supplementary Materials: The following supporting information can be downloaded at: https://www.mdpi.com/article/10.3390/electronics11213530/s1. Figure S1: The dipole antenna scattering parameter S11 calculated by way of the CST-MWS software using both the time domain finite integration technique (FIT) and the finite element method (FEM); Figure S2: The microstrip antenna scattering parameter S11 calculated by CST-MWS using both the time domain FIT and the frequency domain FEM; Figure S3: The radiated electric field of the dipole antenna shown in Figure 2a at a distance of 3 m along the *z*-axis from the center of dipole antenna. Comparison between the full-wave approach and the Huygens' surface approach; Figure S4: The radiated electric field of the three microstrip antennas shown in Figure 7. The distances between the EMI sources and the observation point are 1.5 m; Figure S5: The radiated electric field from the three microstrip antennas shown in Figure 7. (a) Observation point at (0.5, 0, 0). (b) Observation point at (−0.5, 0, 0); Figure S6: The radiated electric field of three dipole antennas in the same configuration as in Figure 7. The distance between the observation point and each EMI source is 10 m; Figure S7: The radiated emission from multiple devices with random phase in the frequency range from 0.8 to 1.2 GHz for 1000 Monte Carlo simulations. (a) For 3 devices, (b) For 9 devices; Figure S8: The radiated emission from multiple devices with random phase and orientation in the frequency range from 0.8 to 1.2 GHz for 1000 Monte Carlo simulations. (a) For 3 devices, (b) For 9 devices; Figure S9: The radiated emission from multiple devices configured in two-dimensional array with random phase in the frequency range from 0.8 to 1.2 GHz for 1000 Monte Carlo simulations. (a) For 3 × 3 devices, (b) For 9 × 9 devices; Figure S10: The radiated emission from multiple devices configured in two-dimensional array with random phase and orientation in the frequency range from 0.8 to 1.2 GHz for 1000 Monte Carlo simulations. (a) For 3 × 3 devices, (b) For 7 × 7 devices; Table S1: The radiated emission from a linear array of EMI sources at a minimum distance of 3 m from the devices at 0.8 GHz. The radiated emissions for the correlated case study are provided for comparison purposes in the first column; Table S2: The radiated emissions from a linear array of EMI sources at a minimum distance of 3 m from the devices at 0.9 GHz. The radiated emissions for the correlated case study are provided for comparison purposes in the first column; Table S3: The radiated emissions from a linear array of EMI sources at a minimum distance of 3 m from the devices at 1.1 GHz. The radiated emissions for the correlated case

study are provided for comparison purposes in the first column; Table S4: The radiated emissions from a linear array of EMI sources at a minimum distance of 3 m from the devices at 1.2 GHz. The radiated emissions for the correlated case study are provided for comparison purposes in the first column; Table S5: The radiated emissions from a two-dimensional linear array of EMI sources at a minimum distance of 3 m from the devices at 0.8 GHz. The radiated emissions for the correlated case study are provided for comparison purposes in the first column; Table S6: The radiated emissions from a two-dimensional linear array of EMI sources at a minimum distance of 3 m from the devices at 0.9 GHz. The radiated emissions for the correlated case study are provided for comparison purposes in the first column; Table S7: The radiated emissions from a two-dimensional linear array of EMI sources at a minimum distance of 3 m from the devices at 1.1 GHz. The radiated emissions for the correlated case study are provided for comparison purposes in the first column; Table S8: The radiated emissions from a two-dimensional linear array of EMI sources at a minimum distance of 3 m from the devices at 1.2 GHz. The radiated emissions for the correlated case study are provided for comparison purposes in the first column.

Author Contributions: Conceptualization, H.K., C.P., E.d.R., P.K., M.R. and F.R.; software, H.K.; validation, H.K.; writing—original draft preparation, H.K., M.R. and F.R.; writing—review and editing, C.P., E.d.R., P.K. and A.M.; supervision, M.R, F.R., C.P. and P.K. All authors have read and agreed to the published version of the manuscript.

Funding: This research was funded by Federal Office of Communications Electromagnetic Compatibility Section, Biel/Bienne, Switzerland, grant number 840001133.

Data Availability Statement: The data that support the findings of this study are available upon reasonable request from the corresponding author.

Conflicts of Interest: The authors declare no conflict of interest.

References

1. Fockens, T.W.H.; Zwamborn, A.P.M.; Leferink, F. Measurement methodology and results of measurements of the man-made noise floor on HF in the Netherlands. *IEEE Trans. Electromagn. Compat.* **2019**, *61*, 337–343. [CrossRef]
2. Matsumoto, Y.; Gotoh, K.; Yamanaka, Y. Interference Aggregation Involving Near-to Far-Field Propagation of Disturbance and its Impact on Emission Limits for Radio Protection. *IEEE Trans. Electromagn. Compat.* **2022**, *64*, 770–778. [CrossRef]
3. *C63.4a-2017*; American National Standard for Methods of Measurement of Radio-Noise Emissions from Low-Voltage Electrical and Electronic Equipment in the Range of 9 kHz to 40 GHz. IEEE: Piscataway, NJ, USA, 2009; p. 133.
4. *CISPR/1446/DC*; International Electrotechnical Commission (IEC): Geneva, Switzerland, 2020.
5. Takahashi, M.; Murakawa, K.; Ohashi, H.; Tokuda, M. Extrapolation of radiated emissions from telecommunication equipment. *IEEE Int. Conf. Commun.* **1996**, *3*, 1462–1466.
6. Häberlin, H. Total Disturbance by many Distributed Isotropic Disturbance Sources. Available online: https://www.iaru-r1.org/wp-content/uploads/2020/05/Total-Disturbance-by-many-distributed-dist.-sources_V7_E_IARU.pdf (accessed on 16 December 2021).
7. Kootz, T.; Kiwull, N. *Impact of an Increasing Number of Devices*; Document CISPR/1397/INF; IEC: Geneva, Switzerland, 2018; pp. 21–35.
8. Ghosh, K.; Zhang, W.; Meiguni, J.; Patnaik, A.; Pommerenke, D.; Sochoux, P.; Rollin, J.; Li, A.; Liu, Q. Growth of Radiated Emission in Multi-Modular Systems. *IEEE Trans. Electromagn. Compat.* **2020**, *62*, 612–616. [CrossRef]
9. Zhang, L.; Yang, H.; Su, X.; Huang, Q.; Rajagopalan, J.; Pai, D.; Hwang, C.; Fan, J. Radio-Frequency Interference Estimation for Multiple Random Noise Sources. *IEEE Trans. Electromagn. Compat.* **2021**, *64*, 358–366. [CrossRef]
10. Balanis, C.A. *Antenna Theory: Analysis and Design*, 4th ed.; Wiley: Hoboken, NJ, USA, 2016.
11. Taflove, A.; Hagness, S.C. *The Finite-Difference Time-Domain Method*, 3rd ed.; Artech House, Inc.: London, UK, 2005.
12. Kunz, K.S.; Luebbers, R.J. *Finite Difference Time Domain Method for Electromagnetics*; CRC Press: Boca Raton, FL, USA, 1993.
13. Harrington, R.F. *Field Computation by Moment Methods*; Wiley-IEEE Press: Hoboken, NJ, USA, 1993.
14. Gibson, W.C. *The Method of Moments in Electromagnetics*, 3rd ed.; Chapman and Hall/CRC: Boca Raton, FL, USA, 2021.
15. Harrington, R.F. *Time-Harmonic Electromagnetic Fields*; IEEE Press: Piscataway, NJ, USA, 2001.
16. CST STUDIO SUITE Learning Edition. 3DEXPERIENCE Edu. Available online: https://edu.3ds.com/en/software/cst-studio-suite-learning-edition (accessed on 18 September 2022).
17. Clemens, M.; Weiland, T. Discrete Electromagnetism with the Finite Integration Technique. *Prog. Electromagn. Res.* **2001**, *32*, 65–87. [CrossRef]
18. Reddy, J.N. *Introduction to the Finite Element Method*, 4th ed.; McGraw-Hill Education: New York, NY, USA, 2019.

19. Karami, H.; Moini, R.; Sadeghi, S.H.H.; Maftooli, H.; Mattes, M.; Mosig, J.R. Efficient analysis of shielding effectiveness of metallic rectangular enclosures using unconditionally stable time-domain integral equations. *IEEE Trans. Electromagn. Compat.* **2014**, *56*, 1412–1419. [CrossRef]
20. Maftooli, H.; Sadeghi, S.H.H.; Karami, H.; Dehkhoda, P.; Moini, R. An Efficient Time-Domain Integral Solution for a Loaded Rectangular Metallic Enclosure With Apertures. *IEEE Trans. Electromagn. Compat.* **2016**, *58*, 1064–1071. [CrossRef]
21. Sadiku, M.N.O. *Monte Carlo Methods for Electromagnetics*; CRC Press: Boca Raton, FL, USA, 2019.
22. Karami, H.; Khalvati, M.R.; Rubinstein, M.; Rachidi, F. *EMC Impact of Disturbances Generated by Multiple Sources*, Lausanne, Switzerland, 2022.